Journal of Earthquake Engineering

Study of a Ground-Motion Simulation Method using a Causality Relationship

Kenichi Nagao[a] & Jun Kanda[b]

[a] Daiwa House Industry, Umeda, Kita-ku, Osaka, Japan

[b] Department of Architecture, Nihon University, Kanda, Chiyoda-ku,
Tokyo, Japan

Accepted author version posted online: 20 May 2014.Published
online: 01 Jul 2014.

PLEASE SCROLL DOWN FOR ARTICLE

Taylor & Francis
Taylor & Francis Group

Study of a Ground-Motion Simulation Method using a Causality Relationship

KENICHI NAGAO[1] and JUN KANDA[2]

[1]Daiwa House Industry, Umeda, Kita-ku, Osaka, Japan
[2]Department of Architecture, Nihon University, Kanda, Chiyoda-ku, Tokyo, Japan

The causality of natural ground motions is evaluated through statistical values for the phase difference. The causality is expressed in terms of the Hilbert transform relationship between the real and imaginary parts of the Fourier transform of the ground motion. We find that ground motions with a shorter duration have a higher degree of causality. Furthermore, we propose a ground-motion simulation algorithm that incorporates causality. The simulated ground motions, compatible with design response spectra, have almost the same spectrum conversion factors as those estimated from natural ground motions.

Keywords Phase Difference; Causality; Response Spectrum; Hilbert Transform; Design Ground Motion

1. Introduction

In designing large and socially important structures such as nuclear power plants or high-rise buildings, dynamic analysis is done by using artificial ground motions compatible with a code-specified design response spectrum. Usually, this spectrum is a 5%-damping acceleration response spectrum. One way to develop such ground motions is to follow these steps: (a) to set the initial Fourier amplitudes and phase angles; (b) take the inverse Fourier transform and obtain the ground motion; (c) check whether the ground motion's response spectrum is nearly equal to the design response spectrum; and (d) if not, increase or decrease the Fourier amplitudes and go back to step (a). This iteration continues until the requirement in step (c) is satisfied at a certain level, e.g., within 1%.

In the procedure above, the Fourier amplitudes F_k and phase angles ϕ_k are defined independently. On the other hand, previous research has pointed out that there is a relationship between the two components. Thrainsson *et al.* [2000] and Thrainsson and Kiremedjian [2002] provided a scatter plot between the Fourier amplitudes and phase differences $\Delta\phi_k$ similar to Fig. 1a. They observed that the relationship was no longer "independent" and explained the relationship based on the method of envelopes [Nigam, 1984]. Boore [2003] obtained similar scatter plots in the relation between the Fourier amplitude and envelope delay. Montaldo *et al.* [2003] compared relationships between the Fourier amplitudes and phase differences of two ground motions of the same earthquake event: one for ground motion recorded at a short distance (similar to Fig. 1a) and the other for ground motion at

Color versions of one or more of the figures in the article can be found online at www.tandfonline.com/ueqe.

(a)   (b)
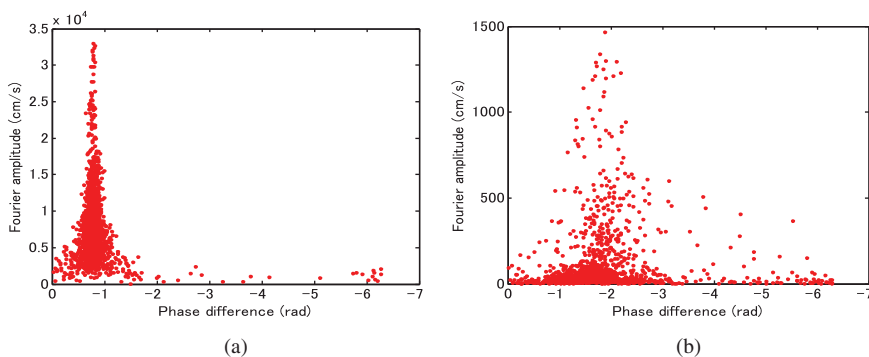
FIGURE 1 Phase differences as a function of the Fourier amplitude for records at a) the Hino site (epicentral distance = 7 km) and b) the Taishi site (epicentral distance = 227 km) from the Tottoriken seibu earthquake (data for 0.1–10.0 Hz are used).

a greater distance (similar to Fig. 1b). They stated that more data points were concentrated at very small amplitudes for the latter case. The two components are expressed as follows:

$$F_k = \sqrt{A_k^2 + B_k^2} \tag{1}$$

$$\Delta\phi_k = \phi_{k+1} - \phi_k \tag{2.a}$$

$$\phi_k = tan^{-1}\frac{-B_k}{A_k} \tag{2.b}$$

where A_k and B_k are the real and imaginary parts, respectively, of the Fourier complex numbers. Therefore, the relationship between the F_k and $\Delta\phi_k$ is essentially represented by a relationship between A_k and B_k. In fact, Papoulis [1977] and Nigam [1982] pointed out that if a ground motion is a causal function, A_k and B_k form Hilbert transform pairs. By using the relationship between A_k and B_k, Sato and Murono [2004] discussed the method to estimate the Fourier amplitudes from the phase angles. However, no one has yet examined quantitatively the relationship between A_k and B_k for natural ground motions. In the present study, the relationship between the real and imaginary parts is evaluated for natural ground motions and an algorithm to simulate artificial ground motion with the same relationship is proposed. This algorithm requires information about the target design spectrum and the mean and standard deviation of the phase differences in certain frequency bands. Furthermore, the advantages of the algorithm are demonstrated by comparing energy characteristics of simulated ground motions satisfying the relationship with those not satisfying it. In the next section, the definitions of causality and phase difference are presented.

2. Definitions

2.1. *Definition of Causality*

In Papoulis [1977], causality is defined as a function of time, *x(t)*, equal to zero for $t < 0$. Therefore, if a function can be expressed as
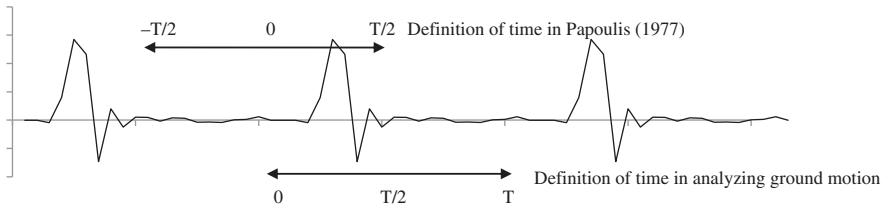
FIGURE 2 Definitions of time history and time shift.

$$x(t) = 0 \quad for\, t < 0 \tag{3}$$

it is a causal function. When taking the Fourier transform for a time history, the real part A_k ($k = -N/2+1, -N/2+2, \ldots, 0, 1, \ldots, N/2$, where $N =$ sample size) and imaginary part B_k ($k = -N/2+1, -N/2+2, \ldots, 0, 1, \ldots, N/2$) are obtained. For causal functions, the A_k relate to the B_k as follows:

$$A_k = \frac{2}{\pi} \sum_{l=-\infty}^{\infty} \frac{B_{k-2l-1}}{2l+1} \tag{4.a}$$

$$B_k = -\frac{2}{\pi} \sum_{l=-\infty}^{\infty} \frac{A_{k-2l-1}}{2l+1} \tag{4.b}$$

Note that the relationship in Eq. (4) is the Hilbert transform for discrete functions.

The discussion above is based on the assumption that the time history is defined for the time domain interval $-T/2 < t < T/2$, where $T = N^*\Delta t$ ($\Delta t =$ time step). On the other hand, when analyzing ground motions, it is usually assumed that the ground motions are defined for $0 < t < T$. Because of this time shift, a ground motion with causality is considered to have zero amplitude after $T/2$; see Fig. 2.

Katukura *et al.* [1989] proposed a symmetrical FFT technique that uses the causality of pulse-like ground motions in the time and frequency domains. In their conclusion, they stated "most of the time functions treated in earthquake engineering are real causal"; hence, the symmetrical FFT technique has wide applicability in the field. However, from the discussion above, it is obvious that ground motions are rarely seen as perfect causal functions. Natural ground motions having a longer duration of strong motion may not be causal functions. Alternatively, even if a ground motion has short strong-motion duration, it may not be a causal function if the large amplitudes appear close to, or after, $T/2$. Therefore, the location of the peak amplitude and duration of the strong motion are important factors for determining the degree of causality in ground motions. The mean and standard deviation of the phase difference, defined in the next section, are useful for quantitative evaluation of the two components.

2.2. Definition of Phase Difference

Ohsaki [1979] defined the phase difference as follows:

$$\Delta\phi_k = \phi_{k+1} - \phi_k \quad (k = 1, 2, \ldots, N/2 - 2) \tag{5.a}$$

$$\phi_k = tan^{-1} \frac{-B_k}{A_k}. \tag{5.b}$$

It should be noted that ϕ is defined for [$-\pi$, π] while the $\Delta\phi$ range is [-2π, 0].

The same author pointed out that the histogram of the phase difference has a shape similar to that of the envelope of the ground motion (see Fig. 3, for instance).

Papoulis [1977], Nigam [1982], and Iwasaki *et al.* [1988] explained the reason by giving a physical meaning for the phase difference. Expressing the ground motion's time history $x(t)$ as a summation of each signal frequency element gives

$$x(t) = \sum_{k=1}^{\frac{N}{2}-1} F_k \cos(2\pi f_k t + \phi_k)$$

$$= F_1 cos(2\pi f_1 t + \phi_1) + \cdots + F_j cos(2\pi f_j t + \phi_j) + \cdots. \tag{6}$$

In Eq. (6), it is assumed that F_0 and $F_{N/2}$ are both zero and they are hence removed from the typical expression of the Fourier transform. Setting all Fourier amplitudes to the same value, F, yields

$$x(t) \approx \cdots + Fcos\frac{1}{2}(2\pi \Delta ft + \Delta\phi_{j-1})cos\frac{1}{2}\left[\left(2\pi f_{j-1} + 2\pi f_j\right)t + \phi_{j-1} + \phi_j\right]$$

$$+ Fcos\frac{1}{2}\left(2\pi \Delta ft + \Delta\phi_j\right)cos\left[\left(2\pi f_j + 2\pi f_{j+1}\right)t + \phi_j + \phi_{j+1}\right] + \cdots. \tag{7}$$

In Eq. (7), each term represents a beat whose envelope and signal frequency are $F_j cos\frac{1}{2}\left(2\pi \Delta ft + \Delta\phi_j\right)$ and $\frac{2\pi f_j + 2\pi f_{j+1}}{2}$, respectively; see Fig. 4. The time t_p at which the beat takes its peak amplitude is calculated as

$$t_p = -\frac{\Delta\phi_j}{2\pi \Delta f} = -\frac{\Delta\phi_j}{2\pi}*N\Delta t. \tag{8}$$

As can be seen from Eq. (8), the phase difference provides the location of the peak envelope of the beat. Hence, the histogram of the phase difference resembles the envelope of the ground motion.

The mean value μ and standard deviation σ can be regarded as the location of the peak amplitude and duration time of strong motion, respectively:
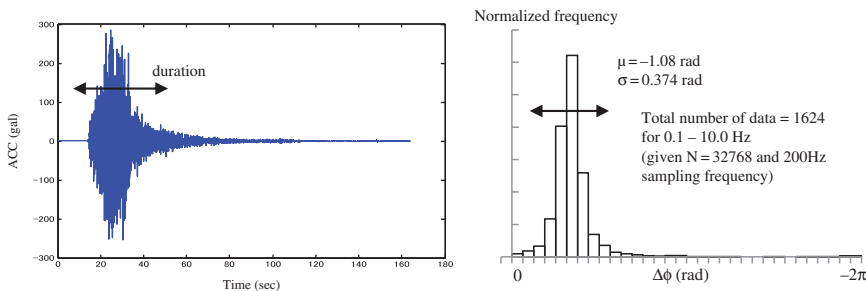
FIGURE 3 Example of ground motion and phase difference distribution.
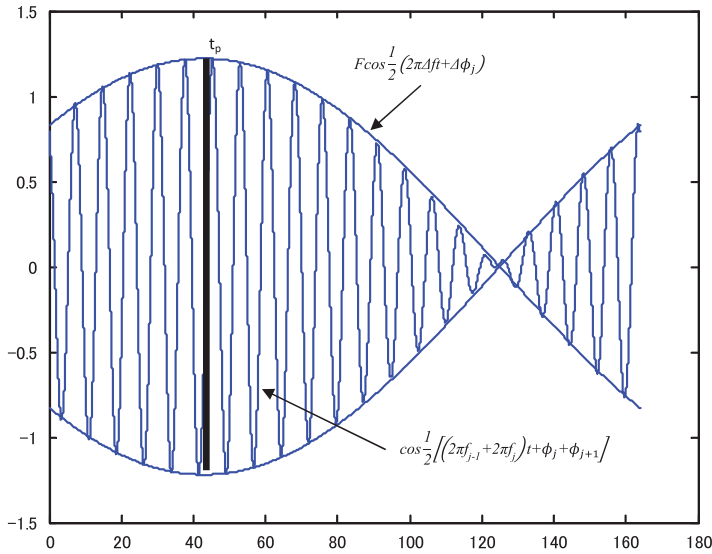
FIGURE 4 Peak location, envelope function, and frequency of the beat.

$$\mu = \frac{1}{N} \sum_{i=1}^{N} \Delta\phi_i \qquad (9.\text{a})$$

$$\sigma = \sqrt{\frac{1}{N} \sum_{i=1}^{N} (\Delta\phi_i - \mu)^2} \; . \qquad (9.\text{b})$$

In computing σ, 2π was added to all phase difference values smaller than $\mu - \pi$, so that all data fall within a range of $\mu \pm \pi$. Nagao and Kanda [2011] showed that the Fourier amplitudes are negligibly small at frequencies where the phase differences are outside $\mu \pm 4\sigma$. Such small values (outliers) sometimes affect σ. Hence, the outliers were eliminated when computing μ and σ (in Nagao and Kanda [2011], approximately 1.6% of all data were judged to be outliers).

The degree to which a ground motion can be seen as a causal function will be influenced by μ and σ. The causality of the natural ground motions is evaluated quantitatively through the following steps.

1. Set all ground motions so that their P-wave motion appears from 15.0 s on the time domain and that the total record length is $N^*\Delta t = 32768^*0.005$ s $= 163.84$ s.
2. For each ground motion, compute μ and σ of phase difference in the following signal frequency bands: 0.1–1.0 Hz, 1.0–2.0 Hz, 2.0–3.0 Hz, 3.0–4.0 Hz, 4.0–5.0 Hz, 5.0–6.0 Hz, 6.0–7.0 Hz, 7.0–8.0 Hz, 8.0–9.0 Hz, and 9.0–10.0 Hz.
3. Take the Fourier transform and compute A_k $(k = 0,1,2, \ldots ,N/2)$ and B_k $(k = 0,1,2, \ldots ,N/2)$ for each ground motion. Then take the Hilbert transform of A_k to obtain $B_k^*(k = 0,1,2, \ldots ,N/2)$. Note that the time shift has already been considered in the definitions of A_k, B_k, and B_k^*.
4. Compute the correlation coefficient between the actual imaginary part, B, and the computed imaginary part, B^*, in each of the frequency bands as follows:

$$\rho = corr\,(B,B^*). \qquad (10)$$

Note that $\rho = 1.0$ means that the ground motion is a perfect causal function. However, ρ does not always become 1.0 for natural ground motion records as will be seen later. The details of ground motion data set are explained in the next chapter.

3. Ground Motion Data Set

After the 1995 Hyogoken-nanbu earthquake in Kobe, Japan's K-NET and KiK-net projects were initiated, and researchers began to utilize the ground-surface and underground acceleration records obtained in a number of earthquakes. Thus, only earthquake events occurring after 1995 are considered. In this study, borehole KiK-net records obtained in fourteen earthquake events, each with M_w is greater than or equal to 6.5, with some exceptions, are used; See Table 1a.

The time step Δt and the sample size N are 0.005 s and 32768, respectively. Thus, ground motions whose record lasts far more than 81.92 s are preferable. If the record length is less than 81.92 s, more than $N/2$ zeros are included in the FFT, causing the ground motion to automatically be a perfect causal function. Only 32 ground motions out of more than 300 records have record lengths less than 163.84 s, with the shortest record length

TABLE 1a Earthquakes' data analyzed in this article

No.	Name	Occurrence date	M_w	Depth	Mechanism	Hypocenter location
1	Tottoriken seibu	2000/10/06	6.6	11 km	Crustal, strike	Long. 133.35 Lat. 35.28
2	Niigataken chuetsu	2004/10/23	6.6	13 km	Crustal, reverse	Long. 138.87 Lat. 37.29
3	Fukuokaken seihouoki	2005/03/20	6.6	9 km	Crustal, strike	Long. 130.18 Lat. 33.74
4	Notohanto oki	2007/03/25	6.7	11 km	Crustal, reverse	Long. 136.69 Lat. 37.22
5	Niigataken chuetsu oki	2007/07/16	6.6	17 km	Crustal, reverse	Long. 138.61 Lat. 37.56
6	Iwate - Miyagi nairiku	2008/06/14	6.9	8 km	Crustal, reverse	Long. 140.88 Lat. 39.03
7	Naganoken-hokubu	2011/03/12	6.7	8 km	Crustal, reverse	Long. 138.60 Lat. 36.98
8	Tokachi oki	2003/09/26	7.9	42 km	Interface, reverse	Long. 144.07 Lat. 41.78
9	Miyagiken oki	2005/08/16	7.1	45 km	Interface, reverse	Long. 142.28 Lat. 38.15
10	Geiyo	2001/03/24	6.7	51 km	Intraplate	Long. 132.71 Lat. 34.12
11	Iwateken nairikunanbu	2001/12/02	6.5	122 km	Intraplate	Long. 141.26 Lat. 39.40
12	Miyagiken oki	2003/05/26	7.0	70 km	Intraplate	Long. 141.68 Lat. 38.81
13	Surugawan	2009/08/11	6.2	23 km	Intraplate	Long. 138.50 Lat. 34.78
14	Miyagiken oki	2011/04/07	7.1	66 km	Intraplate	Long. 141.92 Lat. 38.20

TABLE 1b The number of analyzed records and the minimum and maximum epicentral distances for each earthquake

No.	Name	Min. distance	Max. distance	No. of records
1	Tottoriken seibu	7 km	100 km	33
2	Niigataken chuetsu	15 km	99 km	31
3	Fukuokaken seihouoki	36 km	99 km	22
4	Notohanto oki	35 km	92 km	7
5	Niigataken chuetsu oki	29 km	100 km	23
6	Iwate - Miyagi nairiku	3 km	100 km	38
7	Naganoken-hokubu	16 km	97 km	36
8	Tokachi oki	104 km	150 km	11
9	Miyagiken oki	91 km	148 km	16
10	Geiyo	19 km	98 km	36
11	Iwateken nairikunanbu	8 km	100 km	45
12	Miyagiken oki	13 km	98 km	21
13	Surugawan	21 km	100 km	37
14	Miyagiken oki	83 km	98 km	7

being 120 s. This is the main reason why the KiK-net records were chosen. Acceleration records obtained within 100 km epicentral distance are considered. However, two interface earthquakes occurred off the coast of the Pacific Ocean and the numbers of records within 100 km are very few. For that reason, records up to 150 km for the 2005 Miyagiken oki and 200 km for the 2003 Tokachi oki earthquakes are used. All ground motion records are obtained at underground points where the shear wave velocity, *Vs*, is more than 400 m/s. The number of analyzed records and the minimum and maximum epicentral distances for each earthquake are shown in Table 1b.

4. Causality of Natural Ground Motion

To quantitatively evaluate the degree of causality for the natural ground motion records, the procedures in the "Definition of Phase Difference" section were followed. Before presenting the ρ value of the natural ground motions, the relationships between μ and σ of the phase differences were investigated in each frequency band. Results for 0.1–1.0 Hz and 9.0–10.0 Hz are shown in Fig. 5.

a) 0.1 – 1.0 Hz   b) 9.0 – 10.0 Hz
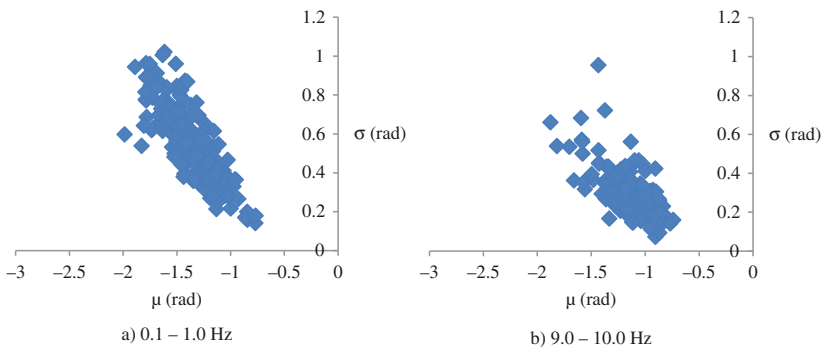
FIGURE 5 Relationship between the μ and σ of the phase difference.

a) 0.1 – 1.0 Hz

b) 9.0 – 10.0 Hz
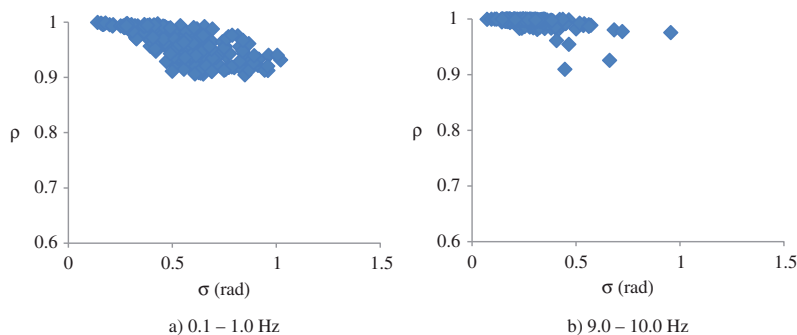
FIGURE 6 Relationship between σ and ρ.

Figure 5 shows that there is a high negative correlation between μ and σ. Therefore, the μ value (the approximate location of the PGA) depends on σ (the duration of the strong motion) in natural ground motions. As stated previously, all ground motions in this study were set so that the P-wave motion appears from 15.0 s. By this setting, the location of PGA can be influenced by the duration of strong motion. For example, relatively delayed PGA is expected for ground motions having a longer duration of strong motion and those ground motions tend to have relatively larger amplitudes after $T/2$, which lowers the ρ values. Note that the ρ value can quantify the degree of causality.

Figure 6 presents the relationship between σ and ρ. Note again that a ground motion with $\rho = 1$ can be seen as a perfect causal function, which is rarely observed in natural ground motions, because minor tremors are usually recorded after $t = T/2$. In Fig. 6, ρ decreases as σ increases, but the relationships are not linear. Moreover, the results in the two frequency bands are similar in terms of both the magnitude of ρ and the rate of decrease.

The criterion to determine whether a ground motion can be considered as causal was chosen as "$\rho \geq 0.95$ in all frequency bands." From the results in Fig. 6, this criterion can be converted to "ground motions having $\sigma \leq 0.65$ rad in all frequency bands." The ground motions satisfying this requirement are called causal ground motions and considered hereafter. The number of records selected in each event was listed in Table 2.

It would be interesting to find out how much of the causality is lost if the phase differences are defined independently of the Fourier amplitudes. To investigate this, artificial ground motions, whose Fourier amplitudes and phase differences were defined independently, were generated by the following procedure. For each of the ground motions in Table 2, rearrange the phase differences randomly with the Fourier amplitudes unchanged in each frequency band. Then compute the phase angles, take the inverse FFT, and synthesize a ground motion. Finally, compute ρ and develop the relationships between ρ and σ. Note that μ and σ were unchanged through the process.

The results for the artificial ground motions and those of the natural ground motions are superimposed in Fig. 7. Note that ρ decreases as σ increases for both types. Moreover, the relationships in the two frequency bands are similar for both types of ground motions. However, the ρ values of the artificial ground motions are smaller than those of the natural ground motions are in the two frequency bands at the same σ values. For instance, ρ value at $\sigma = 0.65$ rad is about 0.80 for the artificial ground motions, whereas $\rho \approx 0.95$ at the same σ for the natural ground motions. Therefore, if the Fourier amplitudes and phase differences are defined independently, the causality is lost unless σ is assumed to be smaller than 0.2 rad considering the criterion.

TABLE 2 The number of records selected as causal functions

No.	Name	No. of records
1	Tottoriken seibu	29
2	Niigataken chuetsu	11
3	Fukuokaken seihouoki	19
4	Notohanto oki	1
5	Niigataken chuetsu oki	2
6	Iwate - Miyagi nairiku	16
7	Naganoken-hokubu	13
8	Tokachi oki	1
9	Miyagiken oki	7
10	Geiyo	32
11	Iwateken nairikunanbu	14
12	Miyagiken oki	12
13	Surugawan	24
14	Miyagiken oki	4
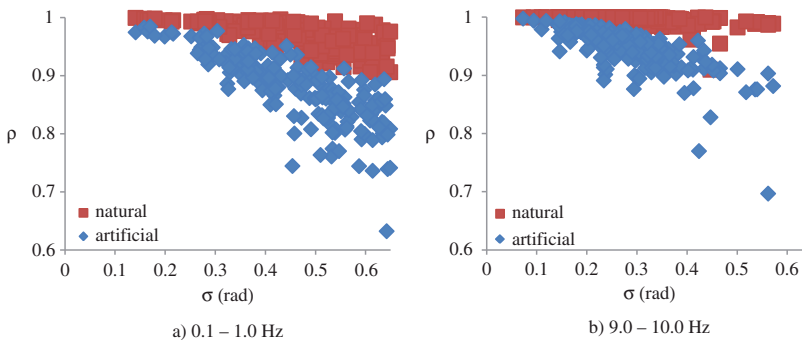
FIGURE 7 Relationship between σ and ρ for natural and artificial ground motions.

5. Algorithm to Develop Causal Ground Motion

In the previous section, the causality of natural ground motions was evaluated. In addition, it was shown that most of the artificial ground motions generated from independent sets of Fourier amplitudes and phase differences might not be considered as a causal function. Here we propose an algorithm to synthesize a causal ground motion, compatible with a design spectrum. To use this algorithm, two kinds of pre-information are necessary. This includes a design spectrum and statistical values (mean and standard deviation) of the phase differences in each of the ten frequency bands. For the design spectrum, a pseudo-velocity response spectrum estimated from Japan's 5%-damping elastic acceleration response spectrum was considered. A different type of spectrum (e.g., 5% damping acceleration response spectrum defined in other countries) can also be used. A procedure to define the statistical values is explained in Nagao and Kanda [2013]. The values are estimated from design presumptions such as magnitude, earthquake type, or source-to-site distance. On the other hand, to show the advantages of the algorithm statistically, using as many sets of realistic μ and σ values as possible will be helpful. For this reason, the sets of μ and σ from natural ground motions in Table 2 are used for the succeeding analyses.

The algorithm consists of the following 12 steps.

1. Define the 5% damping design acceleration response spectrum (DS_a) and μ and σ in the ten signal frequency bands.
2. Set the iteration number, $I = 1$.
3. Define the design pseudo-velocity response spectrum, DS_v, by $DS_a(\omega_n)/\omega_n$, where ω_n = natural circular frequency in rad/s. Further, define the initial Fourier amplitudes, F_I, by multiplying DS_v by $DCF_{\zeta = 0\%}$, the damping correction factor for 0% damping:

$$DCF(f.b., 0) = \frac{mean(S_a(f.b., 0.0))}{mean(S_a(f.b., 0.05))}, \tag{11}$$

where S_a is the absolute acceleration response spectrum and *f.b.* stands for the natural frequency band. Details of this *DCF* are found in Nagao and Kanda [2013]. The initial Fourier amplitudes are defined in the interval 0.05–30.0 Hz, though DS_a and DS_v are defined for 0.1–10.0 Hz. (The $DCF_{\zeta = 0\%}$ outside 0.1–10.0 Hz was estimated by linear extrapolation, whereas DS_v outside 0.1–10.0 Hz was approximated directly using the equation defining DS_a in Japan's code.) It is because response of a structure having a natural frequency, 10.0 Hz, for instance, should be influenced not only by the signal frequency component at 10.0 Hz but also by the signal components at surrounding frequencies. To consider this, the Fourier amplitudes were defined in a broader frequency range than 0.1–10.0 Hz.
4. Generate normal random variables having μ and σ in each of the ten frequency bands. The normal random variables are an initial set of phase difference ($\Delta\phi_{I,k}$, k = 16,17, . . . ,1639). Note that for $N = 32768$ and $\Delta t = 0.005$ s, $\Delta\phi_{I,16}$ is the phase difference at about 0.1 Hz and $\Delta\phi_{I,1639}$ is phase difference at about 10.0 Hz. In step 3, Fourier amplitudes are defined also in the ranges 0.05–0.1 Hz and 10.0–30.0 Hz. The μ and σ values for 0.1–1.0 Hz and 9.0–10.0 Hz are used to generate the initial phase differences for 0.05–0.1 Hz and 10.0–30.0 Hz, respectively. For phase difference data at other frequencies, random variables ranging from -2π to 0 rad are used.
5. Compute the phase angles $\phi_{I,k}$ ($k = 1,2, . . . ,N/2-1$) from the phase differences $\Delta\phi_{I,k}$ using Eq. (5a).
6. ake the inverse Fourier transform and generate the ground motion $X_{I,m}$ ($m = 1,2, . . . ,32768$).
7. Compute the 5% damping velocity response spectrum (denoted $S_{v,I}$) and spectral ratio, a function of frequency, as follows:

$$RS_{I,k} = \frac{DS_{v,k}}{S_{v,I,k}} \quad (k = 16, 17, . . . , 1639) \tag{12.a}$$

$$RS_{I,k} = 1 \quad \text{(elsewhere)} \tag{12.b}$$

8. Multiply F_I by RS_I to obtain F_I'.

$$F_{I,k}' = F_{I,k}^* RS_{I,k} \quad (k = 1, 2, . . . , N/2 + 1). \tag{13}$$

9. Compute the real part $A_{I,k}$ ($k = 1,2, . . . ,N/2+1$) as follows:

$$A_{I,k} = F_{I,k}' * cos(\phi_{I,k}). \tag{14}$$
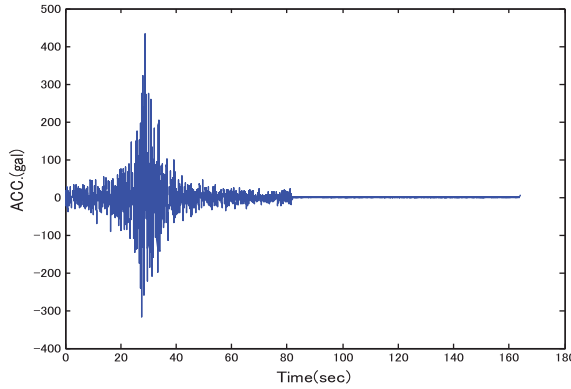
FIGURE 8 Example of simulated causal ground motions.

Then take the Hilbert transform of the real part $A_{I,k}$ to obtain $B_{I,k}^*$ ($k = 1,2, \ldots,$ N/2+1).

10. Update the Fourier amplitudes by

$$F_{I+1,k} = \sqrt{A_{I,k}^2 + B_{I,k}^{*2}}. \tag{15}$$

Then, compute the phase differences by using $A_{I,k}$, $B_{I,k}^*$, and Eq. (2). The phase differences are denoted $\Delta\phi_I'$.

11. Compute the statistical values of $\Delta\phi_I'$ in each frequency band to check whether the $\Delta\phi_I'$ have mean and standard deviation values which are close to those specified in step 1. Usually, the standard deviation values of the $\Delta\phi_I'$ are smaller than the design values specified in step 1 at the first iteration, while the mean values are almost equal. To correct the standard deviation values, the following adjustment is done. For each of the $\Delta\phi_I'$ values in a frequency band,

$$(\Delta\phi_{I+1})_{ith f.b.} = mean\left[\left(\Delta\phi_I'\right)_{ith f.b.}\right]$$
$$+ \left[\left(\Delta\phi_I'\right)_{ith f.b.} - mean\left[\left(\Delta\phi_I'\right)_{ith f.b.}\right]\right] * R_{ith f.b.} \tag{16}$$

where

$$R_{ith f.b.} = \frac{\sigma_{ith f.b.}}{standard\ deviation\left[\left(\Delta\phi_I'\right)_{ith f.b.}\right]} \tag{17}$$

As for the mean value,

$$(\Delta\phi_{I+1})_{ith f.b.} = (\Delta\phi_{I+1})_{ith f.b.} + \left(\mu_{ith f.b.} - mean\left[(\Delta\phi_{I+1})_{ith f.b.}\right]\right) \tag{18}$$

By Eq. (16), each $\Delta\phi_I'$ value is corrected so that the variance of $\Delta\phi_I'$ in the frequency band becomes the same value as σ^2. Due to the adjustment, the intended μ and σ values can be obtained in all frequency bands, as will be seen next.

12. Set $I = I+1$ and go back to step 5. The iteration continues until the difference between unity and mean value of RS_I in Eq. (11a) becomes less than a certain small value. In this study, the value used was 2%. In many cases, this requirement can be satisfied in less than 5-time-iterations.

One example of the simulated causal ground motions is presented in Fig. 8. Note that from 81.92 s ($= T/2$) to 163.84 s ($= T$), all amplitudes are negligibly small. For this ground motion, all $\rho = 1$.

Next, the 5% damping velocity response spectrum, $S_{v,I}$ ($I = 4$ in this case), is compared with the design pseudo-velocity response spectrum, DS_v, in Fig. 9. The $S_{v,I}$ has been converged to the DS_v. Finally, μ, σ, mean, and standard deviation values of the causal ground motion are compared in Table 3. The ground motion has statistical values close to the target statistical values. Thus, simulated ground motions according to the algorithm have the intended μ and σ values, a specific spectral intensity, and causality. Note, however, that the authors recommend using this algorithm only for ground motions expected to have $\sigma \leq 0.65$ rad in all of the 10 frequency bands given $N = 32768$ and $\Delta t = 0.005$ s, as the criterion was defined for the causal ground motion as stated previously.
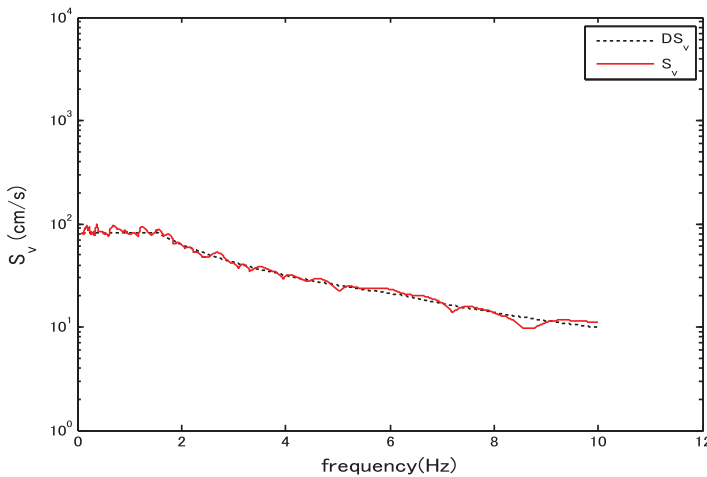
FIGURE 9 S_v and DS_v of the ground motion.

TABLE 3 Target and simulated μ and σ values of the ground motion in Fig. 8

Frequency band	Target μ (rad)	Target σ (rad)	Simulated μ (rad)	Simulated σ (rad)
0.1–1.0 Hz	−1.113	0.279	−1.086	0.282
1.0–2.0 Hz	−1.068	0.222	−1.061	0.227
2.0–3.0 Hz	−1.073	0.219	−1.069	0.222
3.0–4.0 Hz	−1.094	0.198	−1.080	0.215
4.0–5.0 Hz	−1.066	0.265	−1.036	0.275
5.0–6.0 Hz	−1.086	0.205	−1.089	0.215
6.0–7.0 Hz	−1.080	0.209	−1.070	0.219
7.0–8.0 Hz	−1.048	0.168	−1.034	0.166
8.0–9.0 Hz	−1.210	0.326	−1.194	0.340
9.0–10.0 Hz	−1.096	0.211	−1.103	0.214

6. Energy Spectra of Simulated Causal Ground Motions Concept of Energy Spectrum

In this section, the energy spectrum characteristics of the simulated causal ground motions will be discussed. The concept of the energy spectrum, also called the V_E spectrum, was first introduced by Akiyama [1987]. The equivalent velocity, V_E, is represented by

$$V_E = \sqrt{\frac{2E}{m}} \qquad (19)$$

where E is the total energy input to a structure from a ground motion component and m is the mass of the structure.

The response spectrum provides the peak response of all possible linear SDOF systems to a ground motion. On the other hand, the energy spectrum gives the total energy input by a ground motion to all possible linear SDOF systems.

A study of the spectrum conversion factor (*SCF*) between the velocity response spectrum and the energy spectrum can be found in Nagao and Kanda [2014]. The *SCF* is defined as follows:

$$SCF\,(f.b., \zeta) = \frac{V_E(f.b., \zeta)}{S_v(f.b., \zeta)}, \qquad (20)$$

where ζ is the damping ratio.

The simulated causal ground motions are evaluated for their energy characteristics using the following quantities:

$$AV_E = mean\left(\frac{V_E}{DV_E}\right)_{0.1-10.0\,Hz} \qquad (21.a)$$

$$ERR_E = mean\left(\left|1 - \frac{V_E}{DV_E}\right|\right)_{0.1-10.0\,Hz}, \qquad (21.b)$$

where V_E is a 10% damping energy spectrum of the simulated ground motions and DV_E is the expected design energy spectrum defined by $DS_v*SCF(\zeta = 5\%)$. AV_E represents the ratio of the level of V_E to that of DV_E (i.e., the ratio of the simulated energy spectrum to the target energy spectrum), whereas ERR_E gives the mean absolute difference between the two spectra.

Akiyama [1985] observed that damping could smooth the energy spectrum shapes. However, for a damping ratio of more than 10%, the smoothing effect was small. Therefore, he studied the characteristics of 10% damping energy spectrum of natural ground motions. Although DS_v is evaluated for 5% damping, DV_E, the product of DS_v and *SCF*, can be considered also for the 10% damping, because damping is not effective in decreasing the mean energy spectrum level as shown by previous literatures, e.g., Akiyama [1985] and Nagao and Kanda [2014].

7. Effect of Number of Intervals in a Frequency Band

In step 11 of the proposed algorithm, each phase difference value is modified within a signal frequency band so that the mean and standard deviation values can approach the μ and σ defined in step 1. This can also be attained by dividing the signal frequency band into n equal intervals. For instance, consider the target μ and σ values in 7.0–8.0 Hz. If $n = 5$ is

used, each subdivided frequency band, i.e., 7.0–7.2 Hz, 7.2–7.4 Hz, 7.4–7.6 Hz, 7.6–7.8 Hz, and 7.8–8.0 Hz, is supposed to have achieved the target μ and σ values when the iteration is terminated. (The selection of the n value affects the AV_E value significantly, as will be shown next.) The values $n = 1, 2, 3, 4, 5$, and 11 were considered. For all sets of μ and σ of ground motions in Table 2, the AV_E value and ERR_E values were computed for different n. Figure 10 shows the relationship between n and AV_E and n and ERR_E for each of the 185 sets. Note that the thick red line represents the mean AV_E or mean ERR_E for each n value.

Figure 10 shows a tendency for the AV_E value to decrease as n increases, whereas no clear trend can be found in the n-ERR_E relationships. The physical meaning of AV_E suggests that obtaining the value of AV_E closest to unity is preferred. On the other hand, the results of Fig. 10a imply that no specific number of intervals can be suggested to all of the 185 sets of μ and σ values. For some sets of μ and σ, a small n is better, while others require a larger n. Therefore, the authors suggest that for a given set of μ and σ, one should try the smallest n (i.e., $n = 1$), and if too large AV_E is observed, one should increase n to 2, 3, . . . , and so forth, until the AV_E value closest to unity is obtained. The authors' experience indicates that ground motions having relatively small σ values, near-fault pulse-like ground motions, for instance, tend to take a small n value, while those having large σ values will take a large n value.

The AV_E and ERR_E values for the n at which AV_E is closest to unity are noted for each set of μ and σ. Histograms of the AV_E and ERR_E values for the causal ground motions using the 185 sets of μ and σ are shown in Fig. 11.

It can be seen from Fig. 11 that all of the computed AV_E are close to unity and that the mean of ERR_E values is 10.4%. Therefore, the algorithm makes it possible to develop

a) n – AV_E b) n – ERR_E
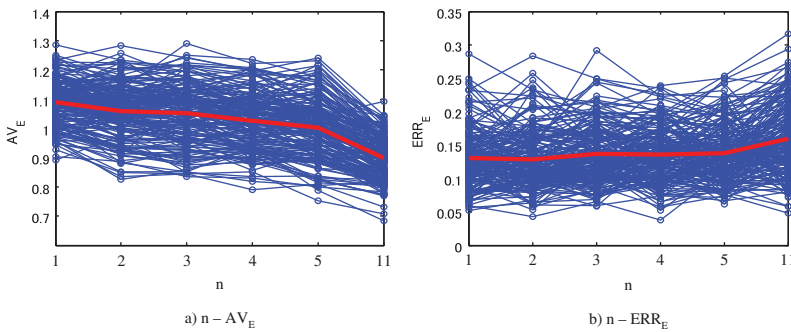
FIGURE 10 Relationship between a) n and AV_E, and b) n and ERR_E.

a) AV_E b) ERR_E
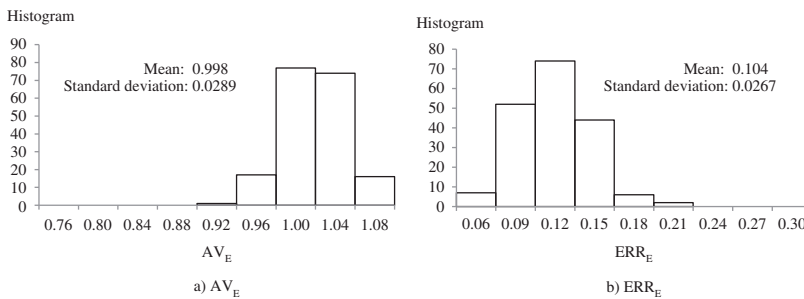
FIGURE 11 Histogram of a) AV_E, and b) ERR_E for simulated causal ground motions.

a) ground motion   b) simulated and target spectra
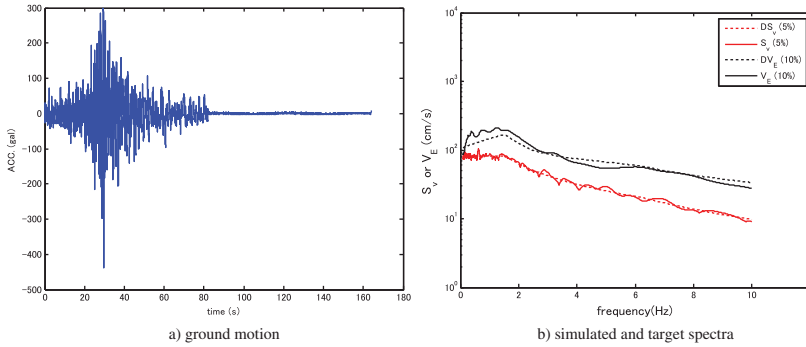
FIGURE 12 Example ground motion and its response and energy spectra ($AV_E = 1.035$ and $ERR_E = 0.115$).

TABLE 4 Set of μ and σ values for ground motion in Fig. 12a

Frequency band	μ (rad)	σ (rad)
0.1–1.0 Hz	−1.51	0.64
1.0–2.0 Hz	−1.286	0.416
2.0–3.0 Hz	−1.062	0.192
3.0–4.0 Hz	−1.088	0.218
4.0–5.0 Hz	−1.106	0.236
5.0–6.0 Hz	−1.107	0.237
6.0–7.0 Hz	−1.099	0.229
7.0–8.0 Hz	−1.09	0.22
8.0–9.0 Hz	−1.081	0.211
9.0–10.0 Hz	−1.073	0.203

a causal ground motion with a design response spectrum and the expected design energy spectrum within a reasonable accuracy.

Figure 12a presents the synthesized ground motion simulated from a set of μ and σ in Table 4. In Fig. 12b, the 5% damping velocity response spectrum and 10% damping energy spectrum with the DS_v and DV_E spectra are shown. It should be noted that the ground motion is causal and the simulated energy spectrum is reasonably well fitted to the design energy spectrum.

8. Comparison to Non Causal Simulated Ground Motions

The 10% damping energy spectrum characteristics of the simulated causal ground motions discussed above are now compared to those computed for non causal artificial ground motions. Note that minor changes are required in the algorithm to develop a non causal ground motion compatible to the design spectrum. These include abbreviations of steps 9 and 10 and changing $F_{I,k}{'}$ and $\Delta\phi_I{'}$ to $F_{I+1,k}$, and $\Delta\phi_{I+1}$, respectively. Also, note that the same *n* value as before was chosen for each of the 185 ground motions in this comparison.

Figure 13 presents the histograms of the computed AV_E and ERR_E values of the simulated non causal ground motions. Figure 13a clearly shows that the non causal AV_E values tend to be smaller than unity by about 15%. In addition, the non causal AV_E values have a
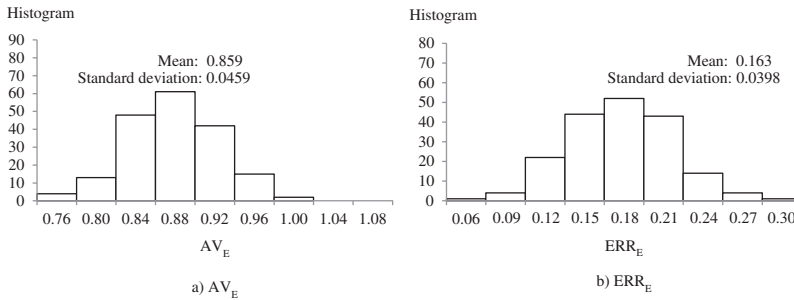
FIGURE 13 Histogram of a) AV_E and b) ERR_E for simulated non-causal ground motions.

larger dispersion (standard deviation = 0.0459) than the causal AV_E values have (standard deviation = 0.0289). From this observation, it can be expected that most of the artificial ground motions compatible with the design response spectrum but not satisfying causality will give less energy to structures than expected. The difference between the energy spectra of the causal artificial ground motions and those of the non causal artificial ground motions comes from the inherent simulation procedures in the algorithm presented in this study. In step 11 of the first iteration, the standard deviation value of the $\Delta\phi'_1$ in each frequency band generally becomes smaller than the target design standard deviation value, σ. Those differences are corrected by Eqs. (16) through (18) to obtain the $\Delta\phi_2$. The new artificial ground motion, X_2, is simulated using the previously updated Fourier amplitudes, F_2, and the updated phase angles, ϕ_2, computed from the $\Delta\phi_2$. The 5% damping velocity response spectrum, $S_{v,2}$, still tends to be smaller than the design response spectrum, DS_v. Note here that if the X_2 is generated from the F_2 and $\Delta\phi'_1$, whose standard deviation values are smaller than those of $\Delta\phi_2$, the 5% damping response spectrum will be very close to the DS_v. Due to the adjustment by Eqs. (16) through (18), the peak amplitude of the X_2 becomes lower as a result of the elongation of the duration of strong motion, causing the smaller response spectrum in the second iteration. Consequently, the spectral ratio in 0.1–10.0 Hz defined by Eq. (12a) still become greater than 1.0, yielding the relatively larger Fourier amplitudes in the causal ground motions (the Fourier amplitude spectrum is equal to the 0% damping energy spectrum, as shown by Akiyama [1985]). The difference between the standard deviation values of $\Delta\phi_I'$ and the target standard deviation values becomes much smaller after the second iteration.

9. Conclusions

1. The causality of the natural ground motions was investigated in terms of the correlation coefficient ρ and it was found that the natural ground motions having $\sigma \leq 0.65$ rad in all ten frequency bands have $\rho \geq 0.95$ in all frequency bands. However, artificial ground motions developed from independent sets of the Fourier amplitude and phase difference have much lower ρ value, i.e., lower causality in all frequency bands.

2. The simulated ground motions generated from the proposed algorithm can have causality, the same spectral intensity as the design response spectrum, and the intended mean and standard deviation values of the phase differences in all frequency bands.

3. The 10% damping energy spectrum of the simulated causal ground motions was compared with the expected design energy spectrum, and the simulated energy spectrum has the same level as the expected energy spectrum.

Acknowledgments

Supplemental Material

Software (coded in MATLAB) used in this study can be provided to researchers and students, for academic use only, by contacting the corresponding author at red-devils-no7@hotmail.co.jp. The authors accept no responsibility for any troubles using the software.

References

Akiyama, H. [1985] *Earthquake-Resistant Limit-State Design for Buildings*, University of Tokyo Press, Tokyo.

Boore, D. M. [2003] "Phase derivatives and simulation of strong ground motions," *Bulletin of the Seismological Society of America* **93**(3), 1132–1143.

Iwasaki, R., Kanda, J., Masao, T., and Ohkawa, I. [1988] "Fundamental properties of phase difference distribution for earthquake ground motions," *Journal of Architectural Institute of Japan* **386**, 16–23 (in Japanese).

Katukura, H., Ohno, S., and Izumi, M. [1989] "Symmetrical FFT technique and its application to earthquake engineering," *Journal of Earthquake Engineering and Structural Dynamics* **18**, 717–725.

Montaldo, V., Kiremidjian, A. S., Thrainsson, H., and Zonno, G. [2003] "Simulation of the Fourier phase spectrum for the generation of synthetic accelerograms," *Journal of Earthquake Engineering* **7**(3), 427–445.

Nagao, K. and Kanda, J. [2011] "Study on the relationship between outliers of phase differences and Fourier amplitude," *Proc. of Japan Conference on Structural Safety and Reliability* **7**, 24–30 (in Japanese).

Nagao, K. and Kanda, J. [2013] "Estimation of damping correction factors using duration defined by standard deviation of phase difference," *Earthquake Spectra*, in press.

Nagao, K. and Kanda, J. [2014] "Spectrum conversion factor and its application for ground motion simulation," *Journal of Japan Association for Earthquake Engineering*, in press.

Nigam, N. C. [1982] "Phase properties of a class of random processes," *Journal of Earthquake Engineering and Structural Dynamics* **10**, 711–717.

Nigam, N. C. [1984] "Phase properties of earthquake ground acceleration records," *Proc. of 8th World Conference on Earthquake Engineering* **2**, 549–556.

Ohsaki, Y. [1979] "Study On the significance of phase content in earthquake ground motions," *Journal of Earthquake Engineering and Structural Dynamics* **7**(5), 427–439.

Papoulis, A. [1977] *Signal Analysis*, McGraw-Hill Co., New York City.

Sato, T. and Murono, Y. [2004] "Simulation of non-stationary earthquake motion based on phase information," *Journal of Japan Society of Civil Engineers* **752**/**I-66**, 159–168 (in Japanese).

Thrainsson, H., Kiremidjian, A. S., and Winterstein, S. R. [2000] "Modelling of earthquake ground motion in the frequency domain," *The John A. Blume Earthquake Engineering Center Report 2000/134*, Stanford University, Stanford, California.

Thrainsson, H. and Kiremidjian, A. S. [2002] "Simulation of digital earthquake accelerograms using the inverse discrete Fourier transform," *Journal of Earthquake Engineering and Structural Dynamics* **31**, 2023–2048.